

Colloidal glass transition observed in confinement

Carolyn R. Nugent,* Kazem V. Edmond, Hetal N. Patel, and Eric R. Weeks†

Physics Department, Emory University, Atlanta, GA 30322

(Dated: November 21, 2018)

We study a colloidal suspension confined between two quasi-parallel walls as a model system for glass transitions in confined geometries. The suspension is a mixture of two particle sizes to prevent wall-induced crystallization. We use confocal microscopy to directly observe the motion of colloidal particles. This motion is slower in confinement, thus producing glassy behavior in a sample which is a liquid in an unconfined geometry. For higher volume fraction samples (closer to the glass transition), the onset of confinement effects occurs at larger length scales.

PACS numbers: 64.70.Pf, 61.43.Fs, 82.70.Dd

Glasses are typically formed by rapidly quenching the temperature of a liquid, resulting in an amorphous liquid-like microstructure with macroscopic solid-like behavior. Upon approaching the glass transition, the temperature might be changed by only a factor of two while simultaneously the viscosity of the liquid grows by many orders of magnitude [1]. A conceptual microscopic explanation for the viscosity growth is the idea of dynamic length scales: in order for molecules in the material to rearrange, they must move together as a group. As the glass transition is approached, the increasing size of these groups relates to the increasing macroscopic viscosity [1, 2, 3, 4, 5, 6].

An important way to probe these length scales is to study the behavior of glass-forming systems when they are confined, to constrict the range of accessible length scales [2, 7, 8, 9, 10, 11, 12, 13, 14]. Intriguingly, the glass transition temperature T_g can be both smaller or larger in confined geometries [11, 12, 13], even for the same material [2, 7, 14]. Experiments and simulations suggest that the interaction between the confining surface and the sample is crucial. For strong interactions (or atomically rough surfaces) the glass transition happens “sooner,” that is, confinement increases T_g by slowing motion near the surfaces [2, 7, 8, 13, 14]. Likewise, for systems that weakly interact with the walls, T_g is typically smaller [2, 7, 11]. However, a clear explanation of these phenomena is still lacking. As it is difficult to get details out of experiments [2], the use of computer simulations to visualize the motion is important [7, 8, 9, 10].

We use confocal microscopy to directly visualize the motion of colloidal particles, which serve as a model system for the glass transition in confinement. Colloids undergo a glass transition in bulk samples as the solid particle volume fraction ϕ is increased [4, 5, 15, 16]. At high volume fraction near the colloidal glass transition ($\phi_g \approx 0.58$), particles move in rearranging groups characterized by a length scale of ~ 3 -6 particle diameters [4, 6], similar to simulations [10]. In this manuscript we study

a mixture of two sizes of colloidal particles confined between two quasi-parallel plates, with a plate gap as small as 3.0 large-particle diameters. In our system confinement induces the glass transition “sooner,” at concentrations for which the bulk behavior is still liquid-like. Studying the glass transition in confinement may help us understand the glass transition in the bulk [2]. Furthermore, understanding the properties of confined liquids has relevance for lubrication [9, 17], dusty plasmas [18], and the flow of glassy complex fluids through microfluidic devices [17].

Our colloidal samples are poly-methyl(methacrylate) particles, sterically stabilized to prevent aggregation [4, 15]. We use a mixture of two particle sizes, with radii $a_{\text{small}} = 1.18 \mu\text{m}$ and $a_{\text{large}} = 1.55 \mu\text{m}$. While the particle polydispersity is low ($\sim 5\%$), the mean particle radii are only known to within $\pm 0.02 \mu\text{m}$. The mixture of two particle sizes prevents crystallization which would otherwise be induced by the walls [8, 18, 19]. In each sample, the small particles are dyed with rhodamine dye, and the large particles are undyed. We use a mixture of cyclohexylbromide and decalin as our solvent, to match the density and index of refraction of the particles; the particles are slightly charged in this solvent [20]. The viscosity of the solvent is 2.25 mPa·s. We examine four different samples A-D, with properties listed in Table I.

We observe our samples using confocal microscopy [20, 21]. As the larger particles are not dyed, we only see the smaller particles. We use a fast confocal microscope (VT-Eye from Visitech, International) with a 63 \times air objective (N.A. 0.70) to scan a volume $50 \times 50 \times 20 \mu\text{m}^3$ once every 2.0 s over a period of an hour. We analyze the images offline to locate the positions of visible (smaller) particles, with a resolution of $0.05 \mu\text{m}$ in x and y (parallel to the walls) and a resolution of $0.1 \mu\text{m}$ in z (parallel to the optical axis). We then track their motion in 3D [20].

Our sample chambers are made by placing a microscope coverslip at a slight angle, supported by a small piece of mylar film (thickness $100 \mu\text{m}$) at one end and resting directly on the microscope slide at the other end [19, 22]. The ends and sides are sealed with UV-curing epoxy. Thus a thin wedge-shaped chamber is formed with an angle $\approx 0.4^\circ$, ensuring that locally the walls are essentially parallel, and allowing us to study a single sample

*Current address: Geophysics and Space Physics, UCLA, Los Angeles, CA

†Electronic address: weeks@physics.emory.edu

TABLE I: Characteristics of the four samples studied. The number ratio $N_{\text{small}}/N_{\text{large}}$ is determined by counting particles in several fields of view using DIC (differential interference contrast) microscopy. The total volume fraction ϕ_{tot} is determined using confocal microscopy, by counting the number of small particles seen in a given imaging volume, using the known number ratio to determine the number of large particles present, and then using the particle sizes and the imaging volume size to compute ϕ_{tot} . Additionally ϕ_{tot} and $N_{\text{small}}/N_{\text{large}}$ was confirmed in samples B–D by direct 3D confocal microscopy observation, where the particle sizes could be easily distinguished and counted; the results were in agreement with the DIC measurements. The volume fractions of the small species and large species, ϕ_s and ϕ_l , are calculated from the other two quantities. The uncertainties of $N_{\text{small}}/N_{\text{large}}$ are $\pm 5\%$, and the uncertainties of ϕ_{tot} are $\pm 8\%$. In particular, note that samples A and C likely do not have the same volume fraction, but it is unclear which has the larger ϕ_{tot} . Samples B, C, and D are prepared by dilutions of one stock sample and thus all have the same $N_{\text{small}}/N_{\text{large}}$.

Sample	$N_{\text{small}}/N_{\text{large}}$	ϕ_s	ϕ_l	ϕ_{tot}
A	3.5	0.26	0.16	0.42
B	3.0	0.13	0.10	0.23
C	3.0	0.24	0.18	0.42
D	3.0	0.26	0.20	0.46

at a variety of different confinement thicknesses [19, 22].

The glass surfaces of the coverslip and slide are untreated. In experiments with sample A, we find that some colloidal particles stick to these surfaces. The stuck particle coverage is typically 10% - 20% of the area. In a second series of experiments done with samples B–D, no particles were stuck. Reassuringly, we find little dependence of the behavior on the number of stuck particles in the results discussed below [23].

For sample A, measuring the positions of the stuck particles allows us to accurately measure the sample thickness. While the uncertainty in locating individual particle positions in z is $0.1 \mu\text{m}$, by averaging data from tens of stuck particles over hundreds of images we locate their mean z position to better than $0.005 \mu\text{m}$. Thus the effective thickness H of each experimental data set is determined to within $0.01 \mu\text{m}$, and is the range in z available to the *centers* of the visible particles. In this manuscript our thicknesses are reported in terms of H . The true surface-to-surface thickness of a sample chamber is found by adding $2a_{\text{small}} = 2.36 \mu\text{m}$ to H .

For the first series of experiments, we study the behavior of sample A ($\phi \approx 0.42$) as a function of thickness. We quantify the particle motion by calculating the mean square displacement (MSD), $\langle \Delta x^2 \rangle = \langle (x_i(t + \Delta t) - x_i(t))^2 \rangle$, where the average is taken over all particles i and all initial times t , and a similar formula applies for $\langle \Delta y^2 \rangle$ and $\langle \Delta z^2 \rangle$. We find that $\langle \Delta x^2 \rangle \approx \langle \Delta y^2 \rangle$ for all our experiments; we report our results for the x direction, the direction over which the sample chamber has constant thickness. We first consider the results for motion parallel to the confining plates, $\langle \Delta x^2 \rangle$, shown in

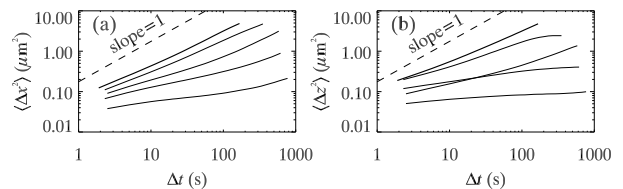


FIG. 1: Mean square displacements. (a) Data for sample A, showing motion parallel to the walls, for thicknesses $H =$ bulk, $16.28 \mu\text{m}$, $11.06 \mu\text{m}$, $9.41 \mu\text{m}$, and $6.92 \mu\text{m}$ (from top to bottom). The dashed line has a slope of 1 and indicates the expected motion for a very dilute bulk suspension of particles with radius a_{small} . (b) Similar to (a), but for motion perpendicular to the walls. Data are ordered by thickness as $\Delta t \rightarrow \infty$, as in (a).

Fig. 1(a). The upper bold line shows motion in an unconfined region and is reproducible for all chamber thicknesses $H > 20 \mu\text{m}$. For this sample, the motion in the unconfined region is nearly diffusive, with the MSD growing almost with slope 1 on the log-log plot. This behavior is similar to monodisperse samples with a volume fraction of $\phi \leq 0.4$ [4]. In other words, this sample is far from the glass transition, $\phi_g \sim 0.6$ [16, 24]. In thinner regions, the motion slows, as seen in the sequence of solid curves below the top bold curve in Fig. 1(a). This slowing starts at a thickness of $H \sim 16 \mu\text{m}$ (2nd curve from top) and slows dramatically for thinner samples; note that Fig. 1(a) shows a log-log plot and thus for the thinnest region shown (bottom curve, $H = 6.92 \mu\text{m}$), to move a distance $\langle x^2 \rangle = (a_{\text{small}}/3)^2$ it takes a time scale 180 times larger than for the bulk region data ($\Delta t = 500 \text{ s}$ as compared to 2.8 s).

These results suggest that confinement induces glassy behavior, with the influence of confinement beginning at $H \approx 16 \mu\text{m} \approx 14a_{\text{small}} \approx 10a_{\text{large}}$ for this sample. For the lower curves in Fig. 1(a), the characteristic behavior of a “super-cooled” sample is seen: at shorter lag times ($\Delta t < 100 \text{ s}$), the MSD has a plateau, while at longer lag times, the MSD begins to rise again [4, 7]. (For short time scales, particles are trapped in cages formed by their neighbors, causing the plateau in $\langle x^2 \rangle$. At longer time scales, these cages rearrange [4, 6].) For the thinnest region (bottom curve), the particles remain localized for the duration of the experiment.

The slowing is also seen in motion perpendicular to the walls, quantified by $\langle \Delta z^2 \rangle$, shown in Fig. 1(b). Moreover, in comparison with Fig. 1(a), it is seen that the motion perpendicular to the walls, $\langle \Delta z^2 \rangle$, is slowed even more so than motion parallel to the walls, $\langle \Delta x^2 \rangle$. This is not surprising, given that particles close to the walls cannot move toward the walls at all, whereas motion parallel to the walls is less restricted.

More than merely constricting motion, the walls also induce a layering of particles, as seen in Fig. 2(a), similar to simulations [8, 25]. The layering is most pronounced immediately adjacent to the walls. The centers of these peaks are not at the precise distance a_{small} from the walls,

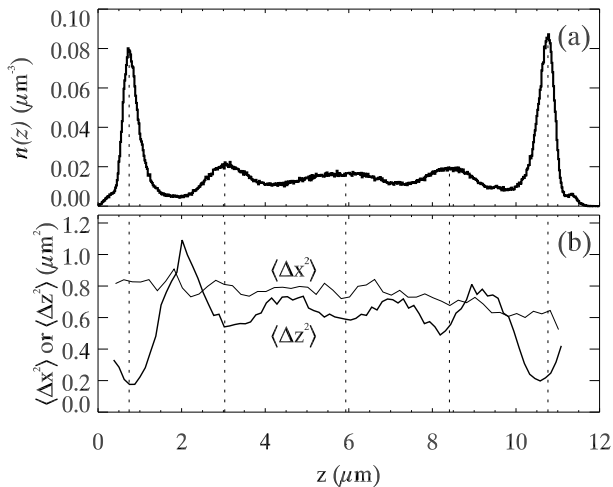


FIG. 2: (a) Particle number density $n_{\text{small}}(z)$ as a function of distance z across the sample cell. Additional particles are stuck to the walls of the sample cell (not shown in the plot) which have centers located at $z = 0.00 \mu\text{m}$ and $z = H = 11.06 \mu\text{m}$. This data corresponds to the middle curve in Fig. 1(a), that is, a sample with moderately slowed dynamics. (b) Mean square displacement parallel to the walls (x) and perpendicular to the walls (z), as a function of z . The displacements are calculated using $\Delta t = 100$ s. The vertical dotted lines indicate the positions of the peaks from part (a). Data shown are from sample A ($\phi \approx 0.42$).

but are slightly offset toward the interior of the sample. (The centers of the stuck particles indicate the maximum possible extent in z that particles could be located, and correspond to the “feet” of the data shown in Fig. 2(a) at $z = 0$ and $11.06 \mu\text{m}$. These particles are not counted in n_{small} shown in Fig. 2(a).)

The layers influence the dynamics, as seen in Fig. 2(b), which shows how $\langle \Delta x^2 \rangle$ and $\langle \Delta z^2 \rangle$ depend on z . The displacements are calculated using $\Delta t = 100$ s, as a representative time scale over which particles begin to move out of this cage, although the results do not depend on this choice and are similar for caged behavior ($\Delta t = 2.0$ s for example). Particles in the layers [the peaks of $n(z)$] have smaller vertical displacements, as seen by the dips in $\langle \Delta z^2 \rangle$ (heavy line). The implication is that particles in layers are in a preferred structure and less likely to move elsewhere [8, 25].

Surprisingly, the layers do not appear to influence the motion parallel to the walls, as seen by $\langle \Delta x^2 \rangle$ (thin line), which does not depend on z . (The slight dip in $\langle \Delta x^2 \rangle$ seen at the largest values of z is not reproducible in other data sets.) This seems counterintuitive as hydrodynamic interactions with the wall normally result in reduced motion for nearby particles [26]. We speculate that the cage dynamics dominate particle motion, rather than hydrodynamic influences [27]. For example, if a particle is pulled by an external force in a direction parallel to the walls, other particles would be forced to rearrange, which is probably the most significant contribution to the drag.

Particle rearrangements would be even more constrained for a particle pulled perpendicular to the wall, thus explaining why we observe slower z motion [27]. Simply put, the high volume fraction likely results in hydrodynamic screening.

Thus while confinement causes the layering of particles near the walls, this layering does *not* appear directly responsible for the slowing of the particle motion. Rather, the layering seems to be an additional influence on the motion in the direction perpendicular to the walls, as seen in Fig. 2(b), but only a minor influence compared to the overall fact of confinement. Note that results do not appear to depend on having an integral number of well-defined layers between the walls [9]. The overall dynamics slow smoothly and monotonically as the confining dimension decreases.

Our observation that the layers closest to the wall have slower motion perpendicular to the walls agrees qualitatively with previous experiments [12, 13, 14] and simulations [7] which suggested that surface layers may be glassier than the interior. However, we note in our experiment this is strongly directionally dependent. The slowing is most easily seen if $\langle \Delta z^2 \rangle$ can be measured independently of the other two directions.

As noted earlier, the growth of dynamic length scales has been observed as the glass transition is approached in a bulk material [1, 2, 3, 4, 5, 6]. For our colloidal samples, this implies that samples with a larger ϕ should exhibit stronger confinement effects. To check this, we took data from samples B, C, and D at various thickness. Qualitatively the data resemble that shown in Fig. 1(a). To capture the H dependence, Fig. 3 shows the values of $\langle \Delta x^2 \rangle$, at fixed $\Delta t = 100$ s, as a function of H for the different samples. Consider the solid triangles, corresponding to sample D. For $H > 50 \mu\text{m}$, $\langle \Delta x^2 \rangle$ is essentially constant. At $H < 50 \mu\text{m}$, the data start showing a strong H dependence, suggesting a confinement length scale of $H^* \approx 50 \mu\text{m}$. For the solid symbols, an increase in H^* is seen as ϕ increases, from approximately $10 \mu\text{m}$ to $50 \mu\text{m}$, confirming that there is a growing length scale as the glass transition is approached. These length scales are significantly larger than those seen for dynamical heterogeneities in monodisperse samples, which are $4 - 8 \mu\text{m}$ [6]. However, this agrees with simulations which found a confinement length scale significantly larger than the mobile cluster size [7]. In Fig. 3, sample A has a smaller value of H^* relative to sample C, which may be due to the excess of small particles in sample A; see Table I.

We find that confinement slows the motion of colloidal particles and thus induces a glass transition to occur sooner than normal, in other words, at volume fractions for which the bulk behavior is liquid-like. Simulations suggest the roughness of the walls is crucial to this slowing [7, 8] and we plan to vary this in future experiments. However, we note that our data show slowing both with completely smooth walls (samples B, C, and D) and walls with isolated stuck particles (sample A). In contrast to our work, rough walls in simulations are composed of

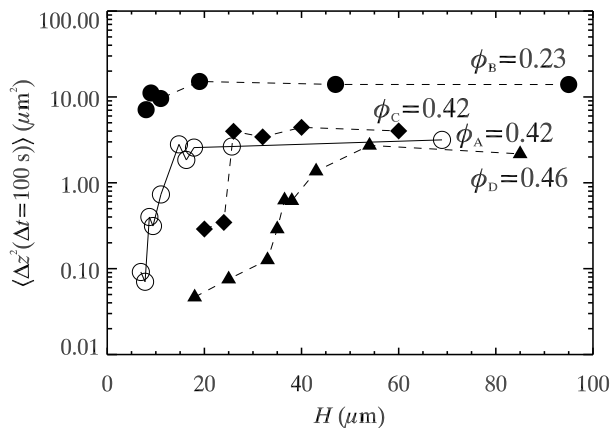


FIG. 3: Value of $\langle \Delta x^2 \rangle$ at $\Delta t = 100$ s, as a function of thickness H , for samples with ϕ as indicated. The open circles correspond to sample A with $N_{\text{small}}/N_{\text{large}} = 3.5$, while the solid symbols correspond to samples B–D with $N_{\text{small}}/N_{\text{large}} = 3.0$. The lines are drawn to guide the eye. The plateau for each data set indicates behavior corresponding to the bulk, whereas the downturn at low H gives an idea of the length scale at which confinement becomes important.

particles fixed in a liquid-like structure [7, 8]. This prevents layering of adjacent particles and restricts motion parallel to the walls. Thus the glass transition in confined samples occurs sooner (at higher temperatures [7] or lower densities [8]). In our experiments, particle motion parallel to the wall is not noticeably inhibited, as seen in Fig. 2. Yet, we still find the glassy behavior occurs sooner: at constant volume fraction, the dynamics are slower as the confining dimension decreases. Thus it seems that the important effect in our experiments is simply the restriction of motion perpendicular to the wall, close to the surface of the wall.

We thank A. Schofield and W. C. K. Poon for our colloidal samples, and J.-L. Barrat, E. R. Dufresne, M. F. Hsu, W. Kob, J. Saldana, and T. M. Squires for helpful discussions. Initial support for this project was provided by the Donors of The Petroleum Research Fund, administered by the American Chemical Society (37712-G7). The work of CRN, KVE, and ERW was also supported by the National Science Foundation under Grant No. DMR-0239109.

-
- [1] C. A. Angell, et al., *J. Appl. Phys.* **88**, 3113 (2000).
[2] M. Alcoutlabi and G. B. McKenna, *J. Phys.: Condens. Matter* **17**, R461 (2005).
[3] M. D. Ediger, *Annu. Rev. Phys. Chem.* **51**, 99 (2000).
[4] E. R. Weeks, et al., *Science* **287**, 627 (2000).
[5] W. K. Kegel and A. van Blaaderen, *Science* **287**, 290 (2000).
[6] E. R. Weeks, J. C. Crocker, and D. A. Weitz, *J. Phys.: Cond. Mat.* **19**, 205131 (2007).
[7] P. Scheidler, W. Kob, and K. Binder, *Europhys. Lett.* **52**, 277 (2000); **59**, 701 (2002).
[8] Z. T. Németh and H. Löwen, *Phys. Rev. E* **59**, 6824 (1999).
[9] P. A. Thompson, G. S. Grest, and M. O. Robbins, *Phys. Rev. Lett.* **68**, 3448 (1992).
[10] K. Kim and R. Yamamoto, *Phys. Rev. E* **61**, R41 (2000).
[11] C. L. Jackson and G. B. McKenna, *J. Non-Cryst. Solids* **131-133**, 221 (1991).
[12] G. Barut, P. Pissis, R. Pelster, and G. Nimtz, *Phys. Rev. Lett.* **80**, 3543 (1998).
[13] J. Schüller, Yu. B. Mel'nichenko, R. Richert, and E. W. Fischer, *Phys. Rev. Lett.* **73**, 2224 (1994).
[14] D. Morineau, Y. Xia, and C. Alba-Simionesco, *J. Chem. Phys.* **117**, 8966 (2002).
[15] P. N. Pusey and W. van Meegen, *Nature* **320**, 340 (1986).
[16] S. I. Henderson, T. C. Mortensen, S. M. Underwood, and W. van Meegen, *Physica A* **233**, 102 (1996).
[17] S. Granick, *Phys. Today* **52**, No. 7, 26 (1999).
[18] L.-W. Teng, P.-S. Tu, and Lin I, *Phys. Rev. Lett.* **90**, 245004 (2003).
[19] C. A. Murray, *MRS Bulletin* **23**, 33 (1998).
[20] A. D. Dinsmore, et al., *Appl. Optics* **40**, 4152 (2001).
[21] V. Prasad, D. Semwogerere, and E. R. Weeks, *J. Phys.: Cond. Mat.* **19**, 113102 (2007).
[22] A. Barreira Fontecha et al., *J. Phys.: Condens. Matter* **17**, S2779 (2005).
[23] We conjecture that the sticking process occurs over a long time period. A year passed between making the first sample chamber and the data acquisition, whereas the second series of samples were investigated within a few weeks of making the sample chambers.
[24] G. Foffi et al., *Phys. Rev. E* **69**, 011505 (2004).
[25] A. J. Archer, P. Hopkins, and M. Schmidt, arXiv:cond-mat/0609663v1 (preprint).
[26] E. R. Dufresne, T. M. Squires, M. P. Brenner, and D. G. Grier, *Phys. Rev. Lett.* **85**, 3317 (2000).
[27] T. M. Squires, private communication.